九州大学学術情報リポジトリ Kyushu University Institutional Repository

Comparative Performance Analysis of a PCM-based Solar Dryer under Natural Air Circulation Conditions

Jamal A.-K. Mohammed

College of Electromechanical Engineering, University of Technology-Iraq

Raed A. Jessam

College of Electromechanical Engineering, University of Technology-Iraq

Louay A. Rasheed

College of Electromechanical Engineering, University of Technology-Iraq

Kamal A. Mohammed

Department of Mechanical Engineering, Mustansiriyah University-Iraq

https://doi.org/10.5109/7363474

出版情報: Evergreen. 12 (2), pp.767-779, 2025-06. 九州大学グリーンテクノロジー研究教育センター

バージョン:

権利関係: Creative Commons Attribution 4.0 International



Comparative Performance Analysis of a PCM-based Solar Dryer under Natural Air Circulation Conditions

Jamal A.-K. Mohammed¹, Raed A. Jessam^{1,*}, Louay A. Rasheed¹, Kamal A. Mohammed²

¹College of Electromechanical Engineering, University of Technology-Iraq, Baghdad,10066, Iraq ²Department of Mechanical Engineering, Mustansiriyah University-Iraq, Baghdad,10052, Iraq

*Author to whom correspondence should be addressed: E-mail: 50097@uotechnology.edu.iq

(Received August 18, 2024; Revised February 05, 2025; Accepted April 01, 2025)

Abstract: The dryer preserves food by using sustainable energy sources like wind and sun. An experimental setup was constructed to evaluate an indirect solar dryer using 50 kg of phase change material (PCM) as a thermal energy storage element. The proposed dryer includes a drying chamber, solar air heater, PCM storage units, a wind turbine ventilator, and a central vertical chimney. This paper aims to compare the performance of a PCM-based dryer under two natural air circulation conditions, one based on the pressure gradient using a chimney (ACP) and the other based on wind ventilation utilizing a wind turbine ventilator (ACW) with an average wind speed of 3m/s. The proposed drying mechanism operates after sunset for 7 to 8 hr under ventilated conditions. The data showed that after using the PCM, the temperature in the chamber is continuously 2 to 7 °C higher than the ambient air. Furthermore, it was observed that the relative humidity of the chamber was 10 to 12.5% lower than that of the ambient air while using the windventilated solar dryer. The PCM-based dryer under the ACW condition has achieved an average drying rate and average collector efficiency exceeding their corresponding values under the ACP condition by about 70.4 % and 24 %, respectively. The proposed dryer is promising due to its lower moisture value and faster drying time.

Keywords: drying chamber; kiwi slices; PCM; solar air heater; solar dryer; wind turbine ventilator

1. Introduction

The sun provides the world with the most energy, known as solar energy, which may be used in two ways: solar thermal and photovoltaic ^{1,2)}. Solar systems are being studied by several researchers to increase heat input, performance parameters, and yield rate^{3–5)}. Solar energy is used for many applications such as drying agricultural products or medicinal herbs.

Drying is the process of removing moisture from agricultural products or medicinal herbs. For long-term storage according to uses, the product's durability has to be improved. Fruits, grains, and vegetables are the main agricultural goods that require preservation. To increase food durability, the majority of crops need to be dried. The material's moisture content is, nevertheless, significantly reduced⁶⁾. Harnessing clean energies such as wind energy or solar energy and its investment in many different applications has become very important in our time. For example, utilizing the waste energy of air conditioners as a

source for electrical power generation via wind turbine⁷⁾. For many years, harnessing the sun's light has been one of the most used methods for drying food goods for preservation. This approach, however, has several drawbacks. It is heavily reliant on environmental factors and requires a sizable surface area as well as prolonged exposure to sunlight. Consequently, the dried product deteriorates⁸⁾. The amount of nutrients in the drying is significantly reduced as a result of direct sunshine and ultraviolet (UV) radiation. Drying is a technique that uses standard energy sources on a commercial scale. There are issues with using this sort of resource, such as environmental damage, source unavailability, expensive transportation costs, etc.

There are many different dryer types available today, but they are not widely used in rural areas because of their high initial costs, ongoing costs, and lack of access to electricity⁹). It's crucial to use renewable energy sources to address these problems, including geothermal, nuclear, wind, biomass, wave, and solar energy. Forced and natural

convection depending on the direction of air movement, solar dryers may be divided into two groups¹⁰⁾. Dryers that use forced convection need fans or blowers that are preferred to be automatically controlled to get high drying efficiency¹¹⁻¹³⁾. Direct, indirect, and hybrid ways of solar drying are further divided into categories.

A material is placed in the insulated container in direct sun dryers. Through a transparent cover, solar energy enters and is absorbed by this material. In indirect dryers, the solar radiation-based heat energy is gathered in separated solar collector (also known as an air heater or solar panel). Then the heated air is delivered to the dryer chamber where the substance is placed. In a mixed-mode drier, heat energy from the sun is directly absorbed by the drying chamber through its transparent walls or roof, while hot air from the attached solar collector is pumped over the material bed¹⁴).

Phase-changing materials (PCMs)^{15,16)} can be categorized as salt hydrates, organic, inorganic, etc. based on other characteristics. The required temperature range determines the process and whether reasonable heat should be used. The key factor in how solar dryers work is storing sensible and latent heat.

Some studies in the literature focused on the issue of designing turbines in ventilation systems, particularly ventilation turbines because these turbines are the most widely used renewable energy options. The solar dryer model utilizes ventilators, which solely rely on the wind impact, to boost airflow. The basic characteristics of a mixed-mode natural-circulation solar dryer are retained by the solar wind-ventilated dryer, with its air circulation system standing out¹⁷). A solar-wind ventilation system is employed to improve the efficiency of the cabinet dryer. To increase buoyancy force, the solar cabinet has a solar flat plate collector and a vertical solar chimney that has been blackened. A smooth-rotating suction axial fan that uses wind power is installed in the chimney¹⁸).

To increase the drying system efficiency, several solar air collectors may be connected in series¹⁹. Thermal energy storage materials are essential for the solar dryer's operation, via improving drying efficiency by emitting heat at night. To use organic PCM with weak thermal conductivity and enhance the rate of heat transfer, the area of these materials might be reduced by increasing their thermal conductivity²⁰. The average efficiency of a solar air heater (SAH) may be raised from 38.7 to 63.35% when it has a built-in storage system for thermal energy made of corrugated tubes filled with paraffin wax²¹. In areas without electricity, solar dryers can be more effective by using a biomass backup heater²².

Using PCM as a thermal storage technology in sun dryers helps save energy since it reduces the time between energy supply and demand²³⁾. It was confirmed by²⁴⁾ that the use of PCM in an indirect solar dryer (ISD) enabled temperatures to reach 2.5 to 7.5 °C above the ambient

temperature for at least 5 hr after sunset. It was claimed in²⁵⁾ that a drying chamber's upper and bottom surfaces coated with paraffin wax allowed for the maintenance of a 6°C temperature greater than the surroundings for 6 hr after sunset which improved the effectiveness of the dryer with mixed mode, although it is superior to other types of solar dryers. When tested under no-load conditions for an indirect mode solar dryer (IMSD) using PCM with forced circulation, it was found that the drying chamber's temperature was maintained at a range of 4 to 16°C higher than the surrounding air²⁶).

Thermo-physical characteristics relevant to the drying of different crops may be identified and presented in a mathematical statistical model with the use of drying kinetics²⁷). The coefficients of the many existing models are affected by the air mass flow rate²⁸⁾. For characterizing the drying process of various crops, the Henderson and Pabis model was determined to be the most appropriate²⁹⁾. Midilli et al. model best described the drying behavior of coriander leaves, via applying a solar dryer with a mixed mode. The five models; the Wang-Singh model, the Logarithmic model, the Midilli et al. model, the doubleterm model, and the improved Henderson and Pabis's model were the most effective options for drying in an IMSD and PCM³⁰). The dryer employed paraffin wax as a PCM, which released latent and perceptible heat after sunset, allowing it to function well for the following 5 hr. Through the use of non-linear regression analysis, XLstat, a statistical analysis tool, was employed to assess the model errors and constant values. Among various models of thin-layer drying properties, the modified Henderson and Pabis model was determined to be the most appropriate for the drying behavior of banana slices³¹⁾.

The ideal tropical solar chimney design was suggested by Alex and Nyuk³²⁾, who also investigated the impact of the solar chimney's stack height, depth, breadth, and intake position on interior performance. According to the testing, the width of the chimney has the greatest impact on output air speed, while the temperature of the output air stays constant. Firfiris et al.333 experimentally assessed many solar chimney designs to dry potato and banana slices, taking into account factors such as material composition and size. According to the experiment findings, the drying rate was comparable to sun drying methods. The height and material properties of the drying tubes, in addition to the meteorological circumstances, were parameters that affected the drying rate. A 40 to 100% increase in flow rate may be attained by increasing the drying tube by 1 m and using the right manufacturing material.

Jessam and Al-Azawiey³⁴⁾ successfully correlated the performance of an SAH to the length and inclination angles. They found that the period from 12:00 to 3:00 p.m. gives the most efficiency with all examined cases. Additionally, it has been proved that the inclination angle has a larger impact on improving SAH performance than does the

passage length. Raed and Han³⁵⁾ studied the use of an external heat source in conjunction with an inclined solar chimney at an average temperature of just 88.0°C. According to the findings, the hybrid model's average improvement in air temperature rise over the solar mode was 33%. Rasheed et al.³⁶⁾ designed an absorption plate with a wire mesh layer in front of a standard SAH. They examined this design and compared its performance to a conventional flat absorber plate. At three values for the mass flow rate 0.05, 0.08, and 0.11 kg/s, an experiment was carried out on a heater. The average thermal efficiency of the flat absorption plate with wire mesh layer method was 53.3, 72.6, and 86.2% with the chosen flow rate values, while it was 42.5%, 57.1%, and 68.1% for the conventional plate.

An indirect-type solar dryer was developed by Alkahdery et al.³⁷⁾ for drying agricultural goods. This dryer has an electric heater that serves as an auxiliary source, an insulated drying chamber, a solar flat plate air collector, and an electric DC fan to enhance the dryer's functionality. Three distinct airflow rates, 0.042, 0.0735, and 0.105 m³/s, were used in the tests. It was shown that the drying chamber's air temperature may be maintained between 32 and 42 °C by employing the auxiliary heater in addition to solar radiation. It was also found that temperature had less impact on dryer effectiveness during the entire drying process at the higher air speeds.

To effectively dry Burmese grapes, Das et al.³⁸⁾ created a novel mixed-mode PCM-based solar dryer (MMSD) with a drying capacity of 15 kg. For three sample types, untreated and blanched at 70°C (BG70) and 80°C (BG80), the system's performance was assessed in two scenarios: inside the solar dryer and outdoors. Drying times were greatly shortened by 5–7 hr with blanching treatments; BG70 had the shortest drying time of 13 hr. BG70 exhibited the highest evaporative heat transfer coefficient of 2.33 W/m²K among the samples.

By adding a PCM to a modified indirect solar flat-plate collector drier (FPSDPCM), Fahim et al.³⁹⁾ implemented a new method for improving the drying of kiwifruit. By obtaining a 38% decrease in drying time and a 10% improvement in thermal efficiency, this study greatly enhanced the drying performance when compared to traditional approaches.

It is evident from the aforementioned literature review that ISDs with energy-storing materials perform better compared with different forms of solar dryers.

This study aims to conduct a comparative experimental analysis of the thermal performance of an ISD using PCM as paraffin wax under two different air circulation conditions: one that uses a chimney and pressure gradient (ACP) and another that uses a wind turbine ventilator (ACW), identifying the best natural air circulation settings to maintain a steady flow of hot air and maintain the drying room's temperature through thermal storage.

During the testing period, some parameters will be considered, such as outlet air temperature and absorption surface temperature of SAH, PCM temperature, relative air humidity and temperature variations of the ambient and inside the chamber, moisture content variations, useful and stored heat rates in SAH, average drying rate, and SAH efficiency.

2. Experimental Setup

The proposed dryer components will be explained below.

2.1. Solar dryer

The development of ventilators that merely rely on the wind impact has increased moisture removal efficiency. The drying chamber, ventilator, and air heating unit of the solar energy dryer with natural circulation are its structural components. The unique feature of this design is that the airflow is controlled by buoyancy forces as well as wind-powered turbine vanes installed on top of the dried attic.

2.2. Solar air heater (SAH)

The SAH equipped with PCM was created locally. A PCM cavity, an absorber, a glass cover, and an insulator make up the SAH. The heater has dimensions of (150 cm \times 90 cm \times 20 cm), as seen in Figure 1. A clear glass cover that was 4 mm thick and with coefficients of emissivity and transmission of 94% and 81%, respectively, was positioned at 0.08 m distant from the absorber. The wax occupies (140 \times 80 \times 5) cm3 of the cavity. As depicted in Figure 2, the absorption plate, a black-coated aluminum sheet 0.001 mm thick, was placed over and in contact with the paraffin wax. The bottom and lateral sides of the SAH were insulated using a 0.05 m layer of Polyurethane with a thermal conductivity of 0.028 W/m.K. Air enters and exits through an opening measuring 6 cm \times 70 cm. The heater is 37° tilted to the horizontal and entirely south-oriented.

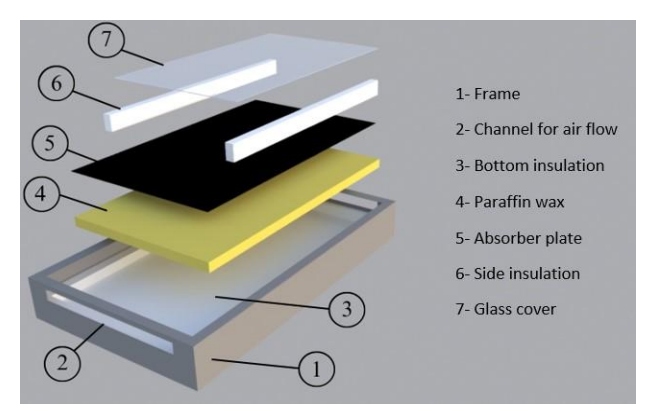


Fig. 1: Schematic of solar air heater



Fig. 2: Absorber plate in contact with paraffin wax

2.3. Drying chamber

The solar drying chamber in Figure 3 has been constructed with measurements of $(1.5 \times 0.87 \times 0.87)$ m3. It comprises a foundation and frame construction made of various materials, thermal insulation, iron sheets, and slots for air to enter and exit through the attic of the test room where the wind turbine ventilator (WTV) is located.

2.4. Solar chimney dryer

The chimney guarantees continuous airflow around the product, thus increasing the speed of drying compared to other designs, so it's a compromise for air circulation between the one that depends on the temperature gradient and another on turbines. The working mechanism is based on the stack effect that occurs in the construction of the solar chimney. The solar circular section chimney, situated on top of the dryer roof, has dimensions of 1 m in height and 13 cm in diameter. Figure 3 shows a schematic illustration of the solar chimney dryer. The dryer is painted in black to absorb solar radiation and raise the temperature of the air passing through the chimney. This raises the buoyant force depending on the temperature differential under investigation.

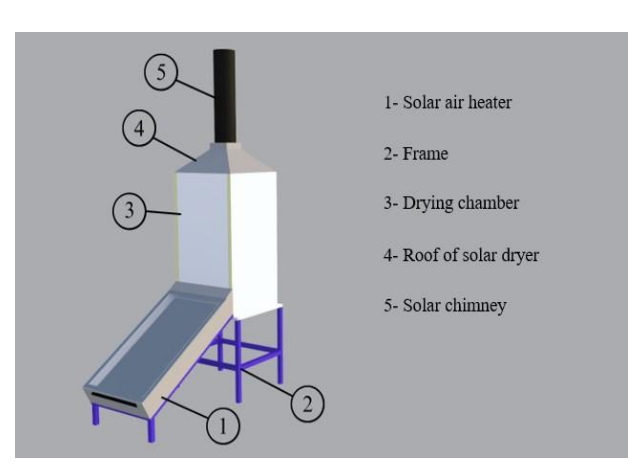


Fig. 3: Schematic of the solar chimney dryer

2.5. Wind Turbine Ventilator (WTV)

Since air flows are essential for natural-circulation solar drying, it is preferable to use WTV with higher and more reliable airflow capacity. The WTV, which is made of steel with the following measurements (width of 25 cm, height of 18 cm, and throat of 13 cm), is put through an experimental test. According to Figure 4, the turbine has 13 bent blades. The WTV is placed on the top of the drying chamber roof shown in Figure 5. The wind turbine's location creates a suction effect that moves air through the chamber. Regardless of the wind direction, the ventilator is employed to function.

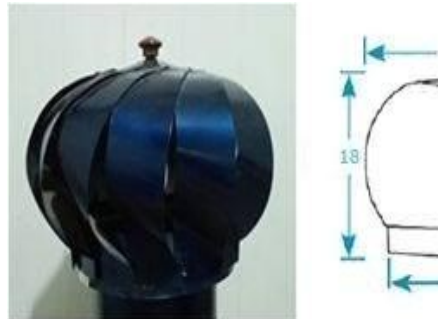


Fig. 4: Wind Turbine Ventilator (WTV)



Fig. 5: Drying chamber

2.6. Using paraffin wax as a PCM

Due to its availability, low cost, chemical stability, and higher storage density than some other materials, paraffin was utilized as a PCM for heat energy storage. The thermophysical properties of the paraffin wax as listed in Table 1.

Table 1: Paraffin wax thermophysical properties⁴⁰.

Properties	Values
Melting Temp.	54 °C
Thermal conductivity "solid"	0.23 W/m.°C
Thermal conductivity "liquid"	0.21 W/m.°C
Latent heat of fusion	190 kJ/kg
Specific heat "solid"	2.0 kJ/kg.°C
Specific heat "liquid"	2.15 kJ/kg.°C
Density of solid	876 kg/m ³
Density of Liquid	795 kg/m ³

3. Experimental Work

Experimental tests were carried out in September 2023 to charge and discharge the SAH in combination with PCM. The tests lasted from sunrise at approximately 7:00 a.m. until sunset at approximately 5:00 p.m. The temperature of paraffin wax will rise above the surface temperature of absorption as solar radiation decreases. As a result, the charging process is finished, and the discharge process continues. In addition to heat transfer from the wax material to the surface of the absorber and subsequently to the air, this is caused by thermal energy stored in the PCM. The examinations were done over two consecutive days, 20 and 21 of Sep., under a clear sky with (33.33 latitude and 44.43 longitude) in Baghdad, Iraq.

The discharge process took place after sunset. As illustrated in Figure 6, on the first day, the dryer was used with a 4 mm thick kiwi slice to store heat energy under chimney air convection conditions, known as pressure gradient-based air circulation (ACP). The second day was carried out using thermal energy storage and wind-powered circumstances, called wind ventilation-based air circulation (ACW). Kiwi slices were used with a weight of 1.4 kg during the two days of the tests and after drying, the weight became 0.37 kg.

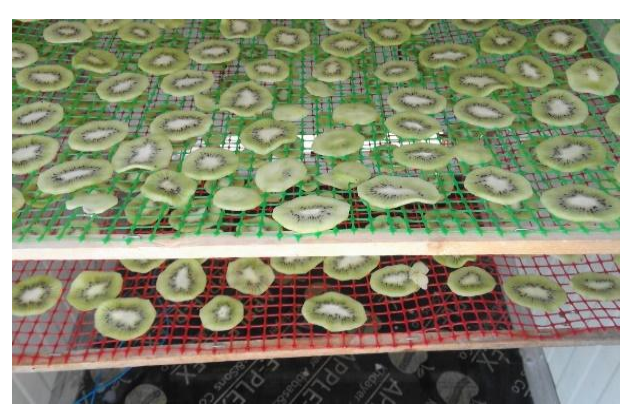


Fig. 6: Kiwi slices to be dried on plastic trays

An ISD functions by putting wet crops on plastic trays inside the drying chamber. To dry the crop, the air entering the chamber must be hot. A solar heater is employed to warm the incoming air. Then the hot air circulates around the wet crop causing the crop moisture to evaporate into the hot air. Variations in the moisture content of the warm air surrounding the surfaces of wet crops result in the production of dry crops.

The base of the drying chamber is connected to the air heater's warm air outlet. Since no special ducting was required, heat losses were reduced and duct insulation was not necessary, saving money. Air flows through the open gap between the SAH's glass cover and absorber plate. The air then enters the drying chamber and is distributed over three perforated plastic trays. Part of the solar light that passes through the transparent cover was absorbed during

the charging process by the black absorption surface of the PCM cavity. The thermal energy that was absorbed was then converted into the SAH's latent and sensible heat forms. The solar dryer with ACP design incorporates a solar chimney to enhance air circulation in the drying chamber. Hot air rises and exits the drying chamber (chimney) through the higher vent, while the cold air enters the vent at the bottom of the collector. Its function is to provide a pressure gradient between its top and bottom ends. By doing so, it increases the buoyancy forces placed on the air stream, resulting in a higher airflow velocity and, thus, a faster rate of moisture removal. On the other hand, the ventilator stack is filled with air as the turbine rotates in the wind. The turbine is suspended on a low-friction ball-bearing system. Even in sporadic winds, the motion keeps the head spinning. Fresh air is brought into the heating system under the cumulative influence of the rotary WTV, where it is heated to a higher temperature and has a substantially higher moisture-carrying capacity. The process of discharging is completed when the wind turbine draws air over the SAH from the PCM cavity during the daytime by using the stored heat (When the absorber surface temperature is lower than the paraffin wax temperature) as well as the times when the sun isn't shining. The product sample was weighed every hour to determine the extent to which the moisture content had dropped. The global components of solar radiation were continuously measured using an SM206-SOLAR solar meter with a reading accuracy of ±5%. Moreover, a Lutron (TM - 903 A) 4-channel temperature data logger has been used to measure the temperatures of the collector inlet and outlet, the absorber plate, the drying chamber inlet and outlet, and the PCM with \pm (0.5% +1°C) accuracy. The relative humidity of the air inside the drying chamber and the ambient air was measured using a TES-1341 HOT-WIRE ANEMOMETER. A UNI-T UT362 anemometer with USB was used to measure the airspeed using the wind speed, of $\pm 3\% + 0.5$. To get an average value of 0.65 m/s, the air departure speed was measured three times at the aperture region above the drying chamber via UNI-T UT362 anemometer with USB. The air mass flow rate can be calculated by using the air density, the aperture's crosssectional area, and the average airspeed. Table 2 contains a list of all the measurement equipment' specifications.

 Table 2: Measuring instruments

Instrument	Accuracy	Range	Resolution
SM206-SOLAR	± 5% of	1-3999	
Solar irradiation	-	W/m²	0.1 W/m^2
meter	reading	(btu)	
Lutron (TM-903 A),	± 0.5% +	- 100 to	0.1 °C
4 channels temp.	± 0.576 +	1300 °C	0.1 C
data logger	I'C	1300 °C	

Lutron HT-3007SD Humidity/Temp. Meter	3% reading + 1% RH., 0 to 50°C	5 to 95 % R.H., ± 0.8°C	0.1% R.H., 0.1 deg.
TES-1341 HOT- WIRE Anemometer relative humidity	±3% RH	10 to 95%	±3% RH
UNI-T UT362 Anemometer with USB	±3%+0.5	2~10 m/s	

4. Theoretical Analysis

Bernoulli's equation is used to calculate the pressure difference between two locations inside the model chamber. The first site is 50 cm under the throat slot, while the second site is precisely under the turbine's throat (circular mouth air exit). The following formula may be used to compute the differential pressure⁴¹.

$$\Delta p = \frac{1}{2}\rho(u_o^2 - u_r^2) + g\rho(Z_2 - Z_1)$$
 (1)

Where $u_r = 0$, $g = 9.81 \text{ m/s}^2$, $\rho = 1.2 \text{ Kg/m}^3$, $Z_1 = 0$ m, $Z_2 = 0.5$ m, $P_2 = P_1 - \Delta p \text{ kN/m}^2$, $P_1 = 101.25 \text{ kN/m}^2$, $V^\circ = A_t u_o$, and $A_t = \pi d^2/4$.

The ventilator's power transmission to the fluid may be computed using the formula⁴²⁾:

$$P_h = V^{\circ} * P_2 \tag{2}$$

The rate of air change per hour can be given as follows⁴³:

$$CR = \frac{v^{\circ} \times 3600}{v_R} \tag{3}$$

Table 3 lists the results of experimental tests performed on the ISD on Sept. 20, 2023, including data on external air wind speed, rotation speed, extraction speed, flow rate, power delivered to the air, and air change rate. External atmospheric wind speed, rotational speed, and air extraction speed have values of 3, 78, and 0.65 m/sec, respectively. Using Eq. (1), and through experiment, it was determined that the airflow rate in the WTV was approximately 0.008 m³/s. The value of the power transferred to the air of the ISD using the WTV was estimated to be around 0.75 kW based on Eq. (2), and the value of the air and air change rate was determined to be equivalent to 25 hr⁻¹ according to Eq. (3).

Table 3: Test results of air turbine on 20 Sep. 2023

Wind speed (m/sec)	3
Rotational speed of WTV (rpm)	78
Air extraction speed (m/sec)	0.65
Air flow rate (m³/sec)	0.008
Power transmitted to the air (kW)	0.75
Air change rate (hr ⁻¹)	25

Any thermal system's fundamental design and functioning can be comprehended through the energy analysis approach. The first law of thermodynamics is applied to the experiment's recorded data. The parameters of the SAH with PCM cavities are derived by formulating the general thermal energy balance equation with the bellow presumptions:

- Long-wavelength radiation, it was assumed that the sky was a black body with a comparable temperature.
- The SAH's working range takes into account all of the air's thermophysical characteristics as constants.
- The cover does not allow any solar radiation to be absorbed.

In the two processes, charging and discharging, the thermal energy balance equation is:

$$Q_A = Q_U + Q_{st} + Q_{los} \tag{4}$$

According to³³⁾, the solar collector's beneficial heat gain may be calculated as follows:

$$Q_u = m_a^o C p_a (T_{oc} - T_{ic}) (5)$$

Where:

$$m_a^o = \rho \ u_a A_d = \rho \ u_o A_t \tag{6}$$

From eq. (6):

$$u_a = \frac{u_o A_t}{A_d} = 0.2 \text{ m/s} \text{ and } m_a^0 = 0.01 \text{ kg/s}$$

During the charging and discharging phases, the stored heat flux is described as¹³):

$$Q_{st} = q_S + L_F + q_L \tag{7}$$

For charging:
$$q_S = m_{PCM}^{\circ} Cp_S (T_F - T_{pcm.i})$$

 $q_L = m_{PCM}^{\circ} Cp_L (T_{pcm.f} - T_F)$
For discharging, $q_L = m_{PCM}^{\circ} Cp_L (T_{pcm.f} - T_F)$
 $q_S = m_{PCM}^{\circ} Cp_S (T_F - T_{pcm.i})$

How much heat is lost is calculated through the following relationship:

$$Q_{los} = U_{los} A_c \left(T_{abs} - T_a \right) \tag{8}$$

There are three basic ways that thermal energy exits the group and the area: convection, radiation, and conduction. The moisture content is calculated using the following equation:

$$M = \frac{W_0 - W_d}{W_0} \times 100 \tag{9}$$

Calculations of useful energy for the dryer come from solar radiation hitting the collector during the day. But when the solar radiation becomes zero, after sunset, input heat energy comes from the PCM as sensible heat until the PCM temperature reaches the ambient temperature. The drying rate can be determined by calculating the difference between initial and equilibrium moisture content via the following proportional relationship⁴⁴):

$$DR = \frac{m_o}{t_d} \tag{10}$$

Heater thermal efficiency with PCM while charging during the day is¹³):

$$\eta_c = \frac{Q_u + Q_{st}}{A_c I} \tag{11}$$

Heater thermal efficiency with PCM while discharging during the night is¹³:

$$\eta_c = \frac{Q_u}{Q_{st}} \tag{12}$$

5. Results and Discussion

Two tests were conducted on two consecutive days under the same climatic conditions with an average wind density of 3 m/s. The necessary readings have been recorded and analyzed. The first day of testing was dedicated to the ISD with PCM under solar chimney (ACP condition), while the second day was for the ISD with PCM driven by wind (ACW condition).

The outside weather conditions for the two successive days are shown in Figure 7. The sun intensity on these two days was determined to be almost identical. The maximum solar radiation intensity with the solar collectors at the inclined plane condition was recorded at 13:00. The values, respectively, were 1180W/m2 under the ACP condition, and 1175 W/m2 under the ACW condition. The ambient temperature reached its maximum at about 14 o'clock, after the sun radiation pattern.

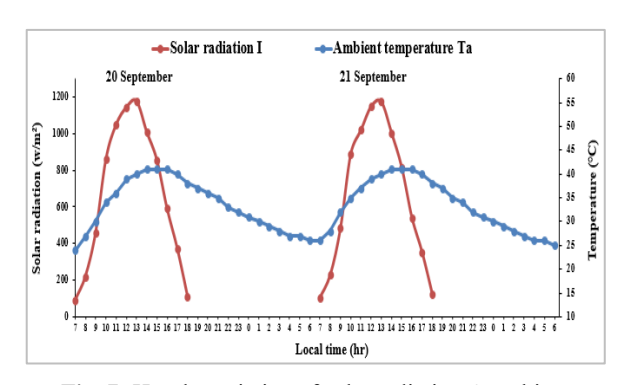


Fig. 7: Hourly variation of solar radiation & ambient temp. (20 & 21 Sep. 2023).

Figure 8 demonstrates the outlet air temperatures variation with SAH in the two conditions of circulation, ACP and ACW; (To.p, To.w), respectively. Particularly during the warmer afternoon hours, the ACP condition's output air temperature is thought to be greater than the ACW condition. This difference is obvious because the air flows

slowly. It depends on the difference in air pressure under the influence of the chimney (air circulation via a pressure gradient). Additionally, as the intensity of solar radiation rises, the outlet air temperature under both circumstances rises over time, reaching its maximum value around 13:00. It then starts to decline until it hits the lowest values around 17:00, which is sunset and continues to decrease after the disappearance of solar radiation until the discharge process ends when the absorption surface temperature becomes equal to the ambient air temperature.

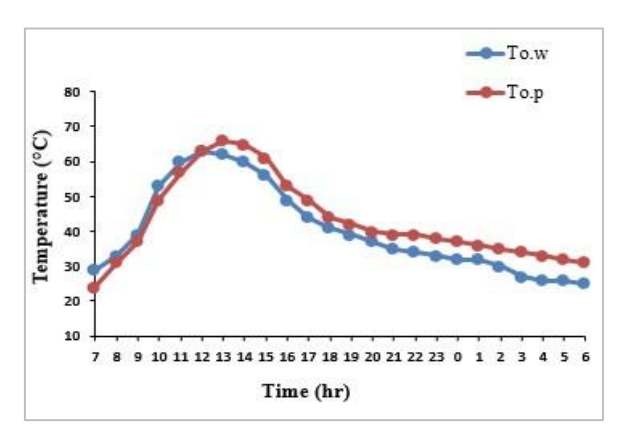


Fig. 8: Hourly variations in outlet air temperature under ACP & ACW conditions (20th & 21st of Sep. 2023)

Figure 9 depicts the variation in PCM temperatures in the SAH under ACP and ACW conditions, (Tpcm.p, Tpcm.w), respectively. The PCM temperature under the ACP state is higher than that under the ACW condition and rises with increasing temperature because heat accumulates throughout the charging process and is not released from it. This is due to the slow mass flow rate of air over the absorption plate because it depends on the pressure gradient only. In addition, the PCM temperature rises to a higher level at 13:00 in both cases as solar radiation intensity increases over time. Then, around 17:00 dusk, it starts to drop to the lowest levels. Until the PCM temperature and the ambient air temperature are equal, the process keeps decreasing.

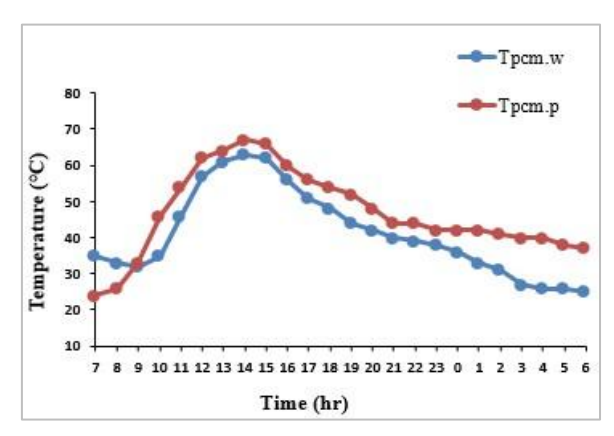


Fig. 9: Hourly variations in PCM temperature under ACP and ACW conditions (20th & 21st of Sep. 2023)

Figure 10 displays the hourly change in the air's relative humidity. Both outside air RHo and inside air RHr in the dryer under the ACP condition had typical relative humidity levels of 12.5% and 20%, respectively. In the ACP condition, the relative humidity of the drying chamber is maximum compared to the relative humidity of the surrounding air. The relative humidity within the drying chamber rises because slow-moving air might not be able to move the water vapor from the product's evaporation to the drier's outside. When the surface is almost completely saturated with moisture, a layer of air is affixed to the surface around this portion of the sliced material. This layer, also known as the border stagnant air layer, slows down the drying process.

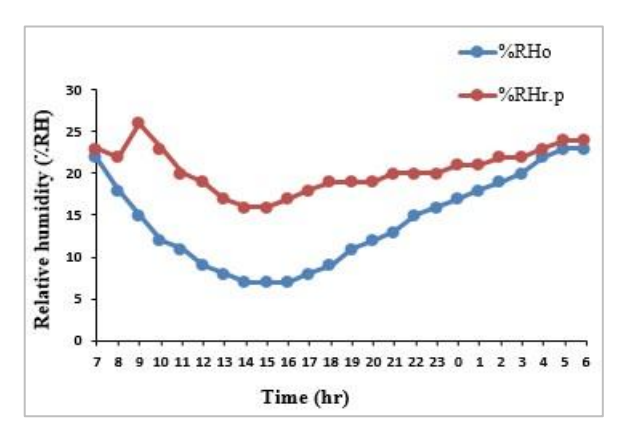


Fig. 10: Hourly variations in relative humidity of ambient air & air inside the chamber under ACP condition

The hourly change in the ambient air's relative humidity is seen in Figure 11. The average value of air relative humidity in the solar dryer with ACW condition and the outside air was 10% and 12.5%, respectively. Air temperature mostly determines relative humidity and is inversely correlated with sun intensity. The high air temperature within the dryer caused its relative humidity to be lower than the ambient air. Between 10 and 18 o'clock, the product dries more quickly because of the larger reduction in relative humidity.

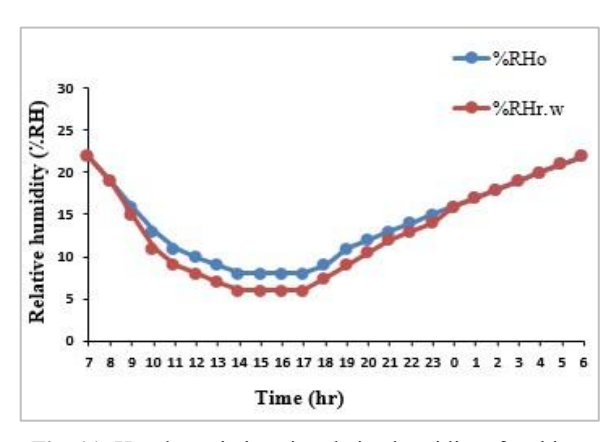


Fig. 11: Hourly variations in relative humidity of ambient air & air inside the chamber under ACW condition

Figure 12 illustrates the temperature change of the absorber surface with PCM under the ACP condition during the day. Until 16:30, the PCM received heat from the top direction of the absorber surface. A little after midday, the heat flow moved from the PCM to the absorber surface. As a result, the ACP condition causes the absorbent surface to overheat since it is involuntary circulated air over it; as a result, no cooling mechanism occurs. The shift in heat flow direction suggests that heat was first stored in the PCM until the height of the sun's rays, after which it was gradually released back onto the absorber surface at a rather constant rate.

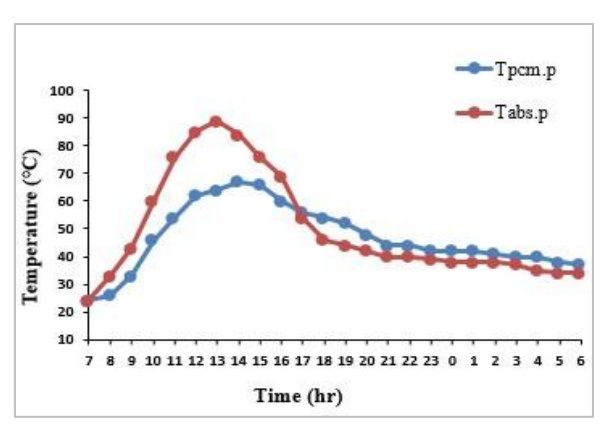


Fig. 12: Hourly temperature variations of PCM-based absorber surface under ACP condition

In Figure 13, the PCM-based absorber surface temperature during the day. Until 14:30, the heat flowed from hot air (ACW condition) to the PCM. After midday, the heat flow shifted from the PCM to the absorber surface. This shift in heat flow's direction suggests that heat was first stored in the PCM until a stored heat was released back onto the absorber surface at a rather steady rate. When the temperature goes up over its melting point of 54 °C, the heat energy is stored as latent heat. The PCM started to release stored latent heat when the temperature of the surface absorber dropped below the PCM melting point. This heat contributed to the dryer's ability to keep a improved consistent temperature, which performance and cut down on the amount of time food needed to dry.

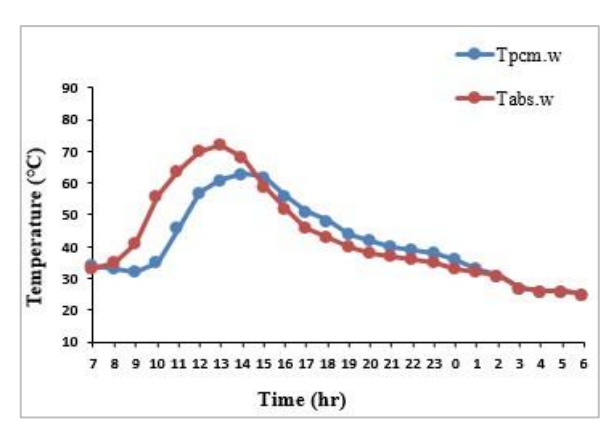


Fig. 13: Hourly temperature variations of PCM-based absorber surface under ACW condition.

Figure 14 shows the relationship between drying time and moisture content under ACP and ACW conditions. The drying curve starts with a phase where the drying rate is constant and ends with a phase where the drying rate decreases. It is clear that before drastically decreasing at the beginning of the drying curve, the drying rate is constant.

When Kiwi slices are exposed to ACW ventilation, moisture will be continually pushed from the inside of the slice to the surface to preserve the moisture pool, where it will evaporate as air flows over the surface. However, the surface moisture pool will quickly disappear. Next, the dryer will start a slower drying stage that requires moisture movement from the heart of the material to its surface. After 6 hr of sunset, the humidity content decreases from the initial value of 0.85 to the final value of 0.11 under the ACW condition, while under the ACP condition, after 14 hr after sunset, the moisture content with 0.85 % will decrease to the final value of 0.13.

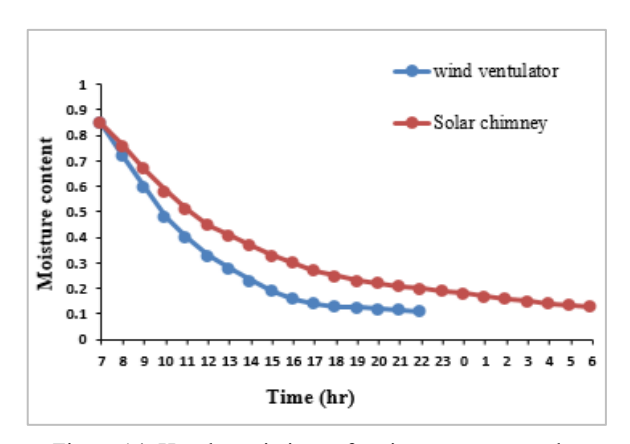


Figure 14: Hourly variations of moisture content under ACP and ACW conditions

Figure 15 depicts the variations in the stored and useful heat rates over two days, 20 and 21 Sept. 2023, for the ACP and ACW conditions. Positive and negative signs on the y-axis indicate the quantity of heat that has been stored. The PCM cavity held a substantial portion of the solar heat that was absorbed. Under ACP and ACW conditions, the

instantaneous heat that accumulates during the first charging period rises with sun radiation and reaches its maximum value at midday, at 0.227 kW and 0.185 kW, respectively. This discrepancy in values is caused by the fact that, in the ACW condition, a significant portion of the heat that was absorbed by the solar radiation (during the charging process) was transferred to the air stream in the SAH as useful heat (up to 0.24 kW), while the remaining portion was stored in paraffin. In the ACP condition, however, there was a slight variation because of the pressure gradient and involuntary air movement through the SAH.

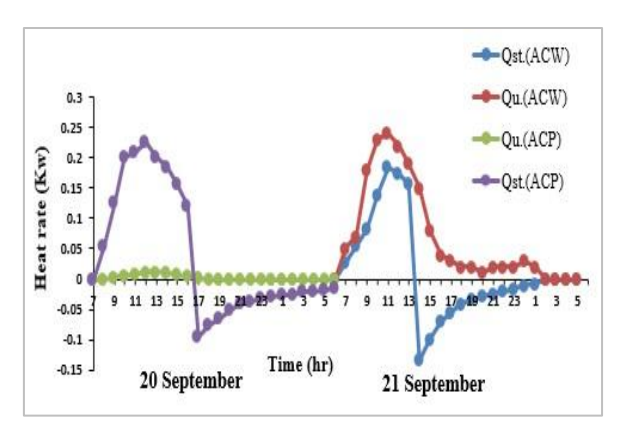


Fig. 15: Hourly variations of useful and stored heat rates in solar accumulator under ACP and ACW conditions

Figure 16 and Figure 17 show the hourly changes in temperature of ambient as well as the air inside the drying chamber with PCM under the ACP and ACW conditions, respectively. It was found that ambient temperature ranges from 26 to 41 °C in both drying conditions.

The air temperature inside the drying chamber is greatly affected by the ambient temperature and sun radiation. This is because the hot drying air is brought and heated by sunlight in the ACW condition, while it is not pulled out and depends only on the pressure gradient (air circulation by pressure difference) in the ACP condition.

When the solar radiation falls, the temperature of the ambient and inside the drying chamber will drop. In the ACP condition, the drying chamber temperature peaked at 52 °C, whereas in the ACW condition, it reached 47 °C.

The air within the drying chamber of the solar dryer underneath the two conditions is warmer at night than the surrounding air. The air within the drying chamber is kept warmer than the ambient temperature by the solar collector due to the nighttime temperature differential, which varies between 2 and 10 °C.

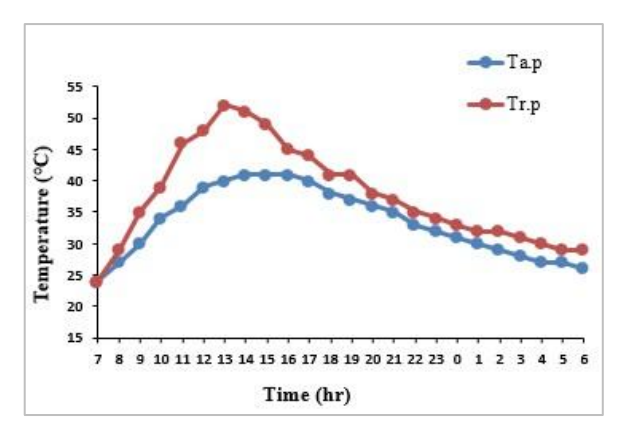


Fig. 16: Hourly variations in ambient temperature and interior drying chamber air temperature under ACP condition

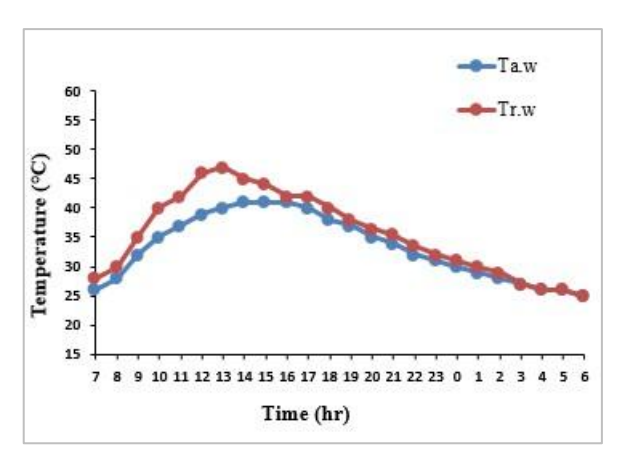


Fig. 17: Hourly variations in ambient temperature and interior drying chamber air temperature under ACP condition

Figure 18 compares average drying rates with the aid of PCM under the two drying conditions. Drying conditions and treatment of products often affect drying time. Under the ACP and ACW conditions, the average drying rates rose to 0.0317 and 0.054 kg/h, respectively, indicating better drying rates. Since it uses the wind turbine ventilator, the PCM-based dryer under ACW produces the maximum drying rate.

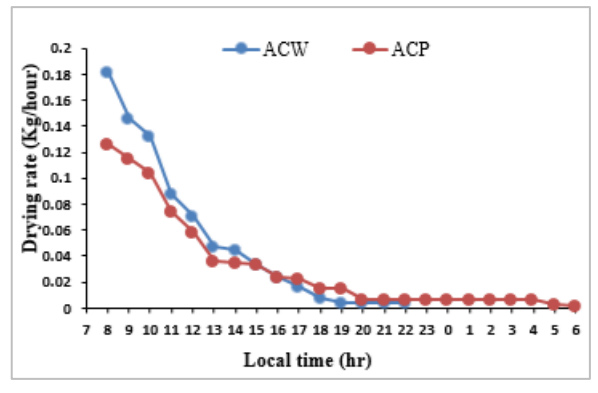


Fig. 18: Hourly average drying rates under drying conditions

It is noted from Figure 19 that the collector's efficiency is often higher in the condition of ACW compared to the ACP one. It should also be noted that under the two drying conditions, the efficiency of PCM assembly increases over time. The same applies to thermal efficiency as it reaches almost its first peak in the middle of the day and the second peak in the evening when the solar radiation decreases sharply and the main heat is provided by the storage system. The use of PCM will increase the efficiency of the air heater, as additional energy stored in the morning will be released during the evening. The figure proves that the PCM-based SAH under the ACP condition has better average collector efficiency than the ACW condition, where the average efficiency was 25 and 31 %, respectively.

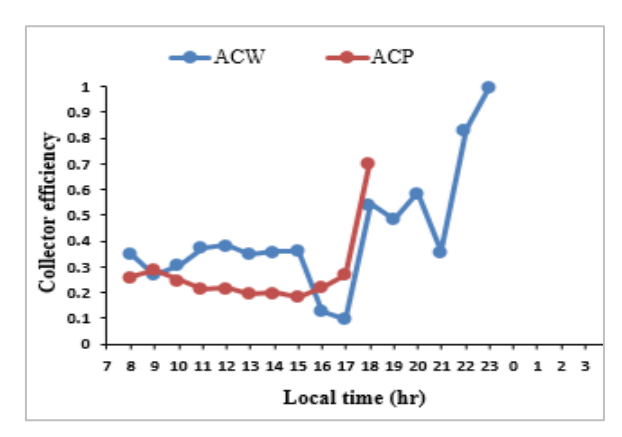


Fig. 19: Hourly collector efficiency under drying conditions

6. Conclusions

Through observing the procedural steps of the experiments and the findings obtained, the following conclusions can be drawn:

It was shown that wind-powered ventilation was more effective and practical than chimney-based pressure gradient ventilation in terms of PCM melting point temperature, moisture sweep, and suitability for the temperature range of the solar food dryer.

During the drying phase, latent heat storage assisted in maintaining a high drying air temperature since the process of releasing heat from the wax to the absorbent surface started around 14:30.

The ideal temperatures of drying air have been achieved in the range (30 - 55) °C under the ACW condition. To keep the product from forming a stagnant air layer, it is crucial to provide continuous chamber air exchange circulation and steam extraction from the drying process.

• 14 hr after sunset, the moisture content decreased by 84.71% due to the heat storage of the PCM-based dryer under ACP condition, while after 6 hr, the reduction rate was 87.1% under ACW condition.

Under ACW condition, the PCM-based dryer has achieved

an average drying rate and average collector efficiency of about 70.4% and 24% higher than their respective values under ACP conditions.

In the future, it is good for charging and discharge behavior to be examined for heat transfer experiments using CFD. Also, the PCM-based solar air collector can be improved as a single-pass solar air heater with adjustments to the absorption plate to enable better performance and comprehensive efficiency of the system, which enhances the quality of the dried product.

Acknowledgments

The authors express their gratitude to the University of Technology's Department of Electromechanical Engineering's Energy and Renewable Energies Branch for providing the technical assistance needed to complete this study.

Nomenclature

$A_{\rm C}$	Area of absorber collector (m ²)
ACP	Natural air circulation based on pressure gradient
ACR	Air change rate
ACW	Natural air circulation based on wind ventilation
A_d	Section area of duct (m ²)
A_t	Cross-sectional area of the throat (m ²)
Cp_a	Specific heat of the air in (kJ/kg. °C)
Cp_L	Specific heat of liquid wax (kJ/kg. °C)
Cp_{PCM}	Specific heat of paraffin wax (kJ/kg. °C)
Cp_S	Specific heat of solid wax (kJ/kg. °C)
d	Diameter of throat (m)
g	Ground acceleration (m/s ²)
hı	Vaporization Latent heat (kJ/kg)
I	Global solar radiation (W/m²)
ISD	Indirect solar dryer
$L_{\rm F}$	Latent heat of fusion (kJ/kg)
m_a^o	Air mass flowrate across the heater in section area
	of duct (m ²)
Qlos	Lost power (W)
Q_{st}	Stored heat energy (W)
Q_U	Useful heat energy (W)
RH	Relative humidity of air (%)
SAH	Solar air heaters
T	Solar drying time (hr)
T_a	Ambient temperature (°C)
T_{abs}	Absorber surface temp. of solar heater (°C)
$T_{\rm F}$	Temperature of fusion (°C)
Tic	Inlet air temperature of SAH (°C)
T_{oc}	Outlet air temperature of SAH (°C)
$T_{pcm.f}$	Final temperature of solid wax (°C)
$T_{pcm.i}$	Initial temperature of liquid wax (°C)
u_a	Air speed inside the duct (m/s)
\mathbf{u}_{r}	Speed of static air inside the chamber (m/s)
u_o	Air extraction speed (m/s)
U_{los}	Overall collector heat loss coefficient (W/m.°C)
DR	Average drying rate (kg/hr)
m_{o}	Moisture mass expelled by solar heat (g)

- $t_{\rm d}$ Overall drying time (hr)
- Thermal efficiency of the solar collector η_c

References

- T.Hanada, Modifying the feed-in tariff system in japan: an environmental perspective, EVERGREEN, 3 (2) 54–58 (2016). https://doi.org/10.5109/1800872
- 2) M. Khanam, M.F. Hasan, T. Miyazaki, B. Baran, and S. Koyama, Key factors of solar energy progress in bangladesh until 2017, EVERGREEN, 5 (2) 78-85 (2018). https://doi.org/10.5109/1936220
- K. Tewari, and R. Dev, Analysis of modified solar water heating system made of transparent tubes & insulated metal absorber," EVERGREEN, 5 (1) 62-72. https://doi.org/10.5109/1929731.
- 4) P. Pal, A.K. Nayak, and R. Dev, A modified double slope basin type solar distiller: experimental and enviro-economic study, EVERGREEN, 5 (1) 52-61 (2018). https://doi.org/10.5109/1929730
- R.A. Rouf, M.A.H. Khan, K.M.A. Kabir, and B.B. Saha, Energy management and heat storage for solar adsorption cooling, EVERGREEN, 3 (2) 1-10 (2016). https://doi.org/10.5109/1800866
- L. Mayor, A.M. Sereno, Modeling shrinkage during convective drying of food materials: a review. J. Eng., (2004)Food 61 373-386. https://doi.org/10.1016/S0260-8774(03)00144-4
- R.A. Jessam, Experimental study of wind turbine power generation utilizing discharged air of air conditioner blower, EVERGREEN 9 (4) (2022) 1103-1109. https://doi.org/10.5109/6625722
- D.R. Pangavhane, R.L. Sawhney, P.N. Sarsavadia, Design, development and performance testing of a new natural convection solar dryer, Energy 27 (6) 579-590. https://doi.org/10.1016/S0360-(2002)5442(02)00005-1
- A. Rajeev, Design, fabrication, installation and field evaluation of 1000 kg capacity solar for chilgoza seed extraction, RERIC Int. Energy J. 20 (2) (1998) 67-75.
- 10) S.K. Natarajan, E. Elangovan, R.M. Elavarasan, A. Balaraman, S. Sundaram, Review on solar dryers for drying fish, fruits, and vegetables, Envir. Sci. Poll. Res. 29 (2022) 40478-40506. DOI: 10.1007/s11356-022-19714-w.
- 11) L.A. Alkahdery, A.V. Yurchenko, J.A.-K. Mohammed, Y.G. Neshina, Automated Temperature and Humidity Control and Monitoring System for Improving the Performance in Drying System, Eurasian Physical **Technical** Journal 20 32-40. (2)(44)(2023)
 - https://doi.org/10.31489/2023No2/32-40.
- 12) L.A. Rasheed, J.A.-K. Mohammed, R.A. Jessam, Performance Enhancement of Solar Air Heater by Integrating Innovative Absorber Design

- Automatic Control Flow Rate, EVERGREEN 10(3)(2023) 1439-1448. https://doi.org/10.5109/7151693.
- 13) L.A.Rasheed, A.V. Yurchenko, V.I. Syryamkin, J.A.-K. Mohammed, Optimization of Agricultural Drying Using PCM Based Automated Indirect Solar Dryers, Russian Physics Journal, 66 (9) (2023) 983-989. https://doi.org/10.1007/s11182-023-03033-9.
- 14) J.O.Ozuomba, N.A. Okonkwo, B.C. Uzor, J.I. Uba, Fabrication and characterization of a direct absorption solar dryer, Adv. Appl. Sci. Res. 4 (3) (2013) 186–194.
- 15) T.K.Murtadha, H.M. Salih, A.D. Salman, Experimental and Numerical Study of Closed Loop Solar Chimney Assisted with PCM and CFM as Thermal Energy Storage Collector, Eng. & Tech. J., 34 (13A) (2016) 2450-2463. https://doi.org/10.30684/etj.34.13A.8
- 16) A.A.Khudhair, F.F. Hatem, D.A.M. Ridha, Enhancement of Thermal Storage Properties of Phase Change Material by Using Metallic Swarf, Eng. & Tech. J. 36 (5A) (2018) 586-595. https://doi.org/10.30684/etj.36.5A.15.
- 17) O.V. Ekechukwu, B. Norton, Review of solar-energy drying systems II: An overview of solar drying technology, Ener. Conver. & Manag. 40 (6) (1999) 615-655.
- 18) M.A. Eltawil, S.E. AbouZaher, W.Z. El-Hadad, Solar-wind ventilation to enhance the cabinet dryer performance for medicinal herbs and horticultural products, CIGR Journal 14 (4) (2012).
- J.M. Jalil, K.F. Sultan, L.A. Rasheed, Numerical and Experimental Investigation of Solar Air Collectors Performance Connected in Series, Eng. & Tech. J. 35 (3A) (2017) 190-196. https://doi.org/10.30684/etj.35.3A.2.
- 20) R.K. Sharma, P. Ganesan, V.V. Tyagi, H.S.C. Metselaar, S.C. Sandaran, Developments in organic solid-liquid phase change materials and their applications in thermal energy storage, Energy Conver. & Manag. 95 (2015) 193–228.
- 21) H.E.S. Fath, Thermal performance of a simple design solar air heater with built-in thermal energy storage system, Energy Conver. & Manag. 36 (1995) 989–97.
- 22) B. Bena, R.J. Fuller, Natural convection solar dryer with biomass back-up heater, Solar Energy 2 (2002) 75–83.
- 23) L.M. Bal, S. Satya, S.N. Naik, V. Meda, Review of solar dryers with latent heat storage systems for agricultural products, Renew. & Sustain.e Ener. Reviews 15 (2011) 876–80.
- 24) S.M. Shalaby, M.A. Bek, Experimental investigation of a novel indirect solar dryer implementing PCM as energy storage medium, Ener. Conver. & Manag. 83 (2014) 1–8.

- 25) D. Jain, P. Tewari, Performance of indirect through pass natural convective solar crop dryer with phase change thermal energy storage, Renew. Ener. 80 (2015) 244–50.
- 26) A.E. Khadraoui, S. Bouadila, S. Kooli, A. Farhat, A. Guizani, Thermal behavior of indirect solar dryer: Nocturnal usage of solar air, J. of Clean. Prod. 148 (2017) 37–78.
- 27) T.Y. Tunde-Akintunde, Mathematical modeling of sun and solar drying of chilli pepper, Renew. Ener. 36 (2011) 2139–45.
- 28) F. Chabane, N. Moummi, A. Brima, An experimental study and mathematical modeling of solar drying of moisture content of the mint, apricot, and green pepper, Energy Sources, Part A: Recovery, Utiliz., & Environ. Effects (2019) 1–15.
- 29) K.B. Koua, W.F. Fassinou, P. Gbaha, S. Toure, Mathematical modeling of the thin layer solar drying of banana, mango, and cassava, Energy 34 (2009) 1594–602.
- 30) P.Mall, D. Singh. Comparative study of performance of indirect mode with PCM and mixed mode solar dryer for coriander leaves. Inter. J. Appl. Eng. Resear. 13 (8)(2018) 5909–19.
- 31) D. Singh, P. Mall. Experimental investigation of thermal performance of indirect mode solar dryer with phase change material for banana slices, Energy Sources, Part A: Recovery, Utilization, and Environmental Effects (2020) 1-8. https://doi.org/10.1080/15567036.2020.1810825
- 32) Y.K.T. Alex, H.W. Nyuk, Parameterization studies of solar chimneys in the Tropics. National University of Singapore, Energ. J. 6 (2013) 145-163. http://dx.doi.org/10.3390/en6010145
- 33) V.K. Firfiris, Z.D. Kaffe, S.D. Kalamaras, A.A. Lithourgidis, A.G. Martzopoulou, T.A. Kotsopoulos, A Prototype Passive Solar Drying System: Exploitation of the Solar Chimney Effect for the Drying of Potato and Banana, Appl. Sci. 12 (11784) 2022. https://doi.org/10.3390/app122211784.
- 34) R.A. Jessam and S.S. Al-Azawiey, Experimental and Numerical Investigation to Correlate Passage Length and Inclination to the Performance of Natural Convective Solar Air Heater. J. of Eng. Science and Tech., 2023, 18(6), pp.3047-3061.
- 35) Jessam, Raed A., and Han J. Chua. "Experimental Evaluation of a Hybrid Inclined Solar Chimney for Power Generation." Inter. J. of Ener. Produc. and Manag. 8 (28) 2 (2023) 81-87. https://doi.org/ 10.18280/ijepm.080204
- 36) L.A. Rasheed, J.A.-K. Mohammed, R.A. Jessam, Performance Enhancement of a Single Pass Solar Air Heater by Adopting Wire Mesh Absorber Layer, EVERGREEN, 10 (2) (2023) 880-887. https://doi.org/10.5109/6792883

- 37) L.A. Alkahdery, A.V. Yurchenko, J.A.-K. Mohammed, A.D. Mekhtiyev, Y.G. Neshina, Performance Improvement of solar dryer using an auxiliary heat source under different values of airflow rates, Eurasian Phys. Tech. J., 20 (1)(43) (2023) 42-50. https://doi.org/10.31489/2023No1/42-50
- 38) B. Das, P. Singh, P. Kalita, Performance Evaluation of a Mixed-Mode solar dryer with PCM-based energy storage for efficient drying of Baccaurea ramiflora, Solar Energy 288 (113279) (2025). https://doi.org/10.1016/j.solener.2025.113279
- 39) Fahim Ullah, K. Hasrat, S. Iqbal, S. Kumar, M. Mu, S. Wang, Performance evaluation of improved indirect flat-plate solar collector drier with integrated phase change material for drying kiwifruit (Actinidia deliciosa A. chev.), J. Stor. Prod. Resear. 111 (102551) (2025). https://doi.org/10.1016/j.jspr.2025.102551
- 40) B. Zalba, J.M. Marín, L.F. Cabeza, H. Mehling, Review on Thermal Energy Storage with Phase Change Materials, Heat Transfer Analysis and Applications, Appl. Ther. Eng. 23 (3) (2003) 251-283. https://doi.org/10.1016/S1359-4311(02)00192-8
- 41) E.B. Wylie, V.L. Streeter, L. Suo, Fluid transients in systems, Englewood Cliffs, NJ: Prentice Hall, 36 (1993) 464.
- 42) R. Edwards, Handbook of Domestic Ventilation, Routledge 2005.
- 43) D.W. Bearg, Indoor Air Quality and HVAC Systems, CRC Press 1993.
- 44) A.O. Adelaja, B.I. Babatope, Analysis and Testing of a Natural Convection Solar Dryer for the Tropics, J. of Ener., 2013. https://doi.org/10.1155/2013/479894